RSS-Based Localization of Low-Power IoT Devices Exploiting AoA and Range Information

Li, Xuhong; Leitinger, Erik; Tufvesson, Fredrik

Published in:
54th Asilomar Conference on Signals, Systems, and Computers

DOI:
10.1109/IEEECONF51394.2020.9443542

2021

Document Version:
Peer reviewed version (aka post-print)

RSS-Based Localization of Low-Power IoT Devices Exploiting AoA and Range Information

Xuhong Li*, Erik Leitinger†, and Fredrik Tufvesson*
*Department of Electrical and Information Technology, Lund University, Sweden.
†Signal Processing and Speech Communication Laboratory, Graz University of Technology, Austria
Email: {xuhong.li, fredrik.tufvesson}@eit.lth.se, erik.leitinger@tugraz.at

***Abstract*—We present a localization algorithm for low-power long-range Internet-of-things (IoT) networks, which exploits angle of arrival (AoA) and range information from non-coherent received signal strength (RSS) measurements. In this work, each anchor node is equipped with array antennas of known geometry and radiation patterns. The position of the target node and the path-loss exponent to each anchor are unknown and possibly time-varying. The joint estimation problem is formulated with a Bayesian model, where the likelihood functions are derived from the classical path-loss model and an RSS difference model. A message passing method is then exploited for efficient computation of the marginal posterior distribution of each unknown variable. The proposed algorithm is validated using real outdoor measurements from a low-power wide area network based IoT system in a challenging scenario. Results show that the proposed algorithm can adapt to dynamic propagation conditions, and improve the localization accuracy compared to a method that exploits only single geometric feature. Furthermore, the algorithm scales well in different antenna array configurations, and is compatible with various existing IoT standards.**

I. Introduction

Location-awareness is a key enabler for various emerging applications related to the Internet-of-things (IoT). Existing localization methods applied in IoT scenarios typically build upon features like time-of-arrival (ToA), angle-of-arrival (AoA), or received signal strength (RSS). Among these, RSS-based localization is especially appealing due to its broad support from low-cost technologies, such as the radio frequency identification, Bluetooth Low Energy, and low-power wide area network (LPWAN) [1] technologies like SIGFOX and LoRa. In this work, we focus on RSS-based localization methods, with particular interest in mid- to long-range outdoor scenarios.

To formulate the localization problem, connected IoT devices are classified as a target node of which the location is to be determined and anchor nodes with known locations. In general, target localization using RSS measurements are based on proximity, fingerprinting [2], [3] or ranging [4], [5] methods. Fingerprinting-based localization exploits the unique structure of the spatial distribution of RSS measurements by matching an RSS measurement with pre-acquired RSS measurements (fingerprints) at the positions of interest. The achievable accuracy is related to the density of fingerprints and degrades in dynamic scenarios. RSS-based ranging for localization is another common method. By exploiting the path-loss model (PLM) [5], it is possible to map an RSS measurement to a range estimate, which is further used to infer the target location w.r.t. the anchor coordinates. However, RSS-based ranging can be unreliable under the conditions of imperfect knowledge of path-loss exponent (PLE) and environmental influence. Typically, RSS-based ranging for outdoor IoT localization provide accuracies from one to a few hundred meters [6]. In recent years, the potential of AoA estimation using non-coherent RSS measurements for target localization is explored in some works [7], [8]. Angle information is mostly obtained by using phase coherent antennas, however this is not feasible for IoT networks when maintaining a low system cost. Most of the existing localization methods have in common that they exploit a single geometric feature, as for example range or angle, and are dedicated to short-range and indoor scenarios.

In this work, we propose a massage passing algorithm for target tracking, that exploits both range and angle information from RSS measurements obtained from anchors equipped with non-coherent antenna arrays. To be adaptive to dynamic propagation conditions, the PLE to each anchor is assumed to be unknown and time-varying. The joint estimation of the target location and PLEs is formulated in a Bayesian sense, where the likelihood functions are derived from the classical path-loss model [5] and an RSS difference (RSSD) model [8]. The statistical model is represented with a factor graph which enables the use of message passing for efficient computation of the marginal posterior distribution of each unknown variable. Furthermore, an interacting multiple model (IMM) method is used to resolve the motion uncertainty of the target [9]. The results are validated using real outdoor measurements from an IoT network based on LoRa system.

II. Problem Formulation

We consider the case that a target node is equipped with an omnidirectional antenna and has unknown time-varying state $\boldsymbol{x}_n \triangleq [\boldsymbol{p}_n^{\mathrm{T}}, \boldsymbol{v}_n^{\mathrm{T}}]^{\mathrm{T}} \in \mathbb{R}^{4\times 1}$, $n = 1, \cdots, N$, where $\boldsymbol{p}_n \in \mathbb{R}^{2\times 1}$ is the position and $\boldsymbol{v}_n \in \mathbb{R}^{2\times 1}$ is the velocity. In the area of interest, anchor nodes indexed by $s \in \mathcal{S} \triangleq \{1, \cdots, S\}$ are distributed with known static positions $\boldsymbol{c}_s \in \mathbb{R}^{2\times 1}$ and array orientations ϕ_s. Each anchor node is equipped with A_s directional antennas indexed by $a \in \mathcal{A}_s \triangleq \{1, \cdots, A_s\}$, and the radiation patterns are assumed to be known. At time n, the AoA $\varphi_{n,s}$ (w.r.t. the sth anchor's coordinate system) and the propagation distance $d_{n,s}$ from the target to the center $\boldsymbol{c}_s$ of the sth anchor are defined as $\varphi_{n,s} = \angle(\boldsymbol{p}_n - \boldsymbol{c}_s) + \phi_s$ and

$d_{n,s} = \|\boldsymbol{p}_n - \boldsymbol{c}_s\|$. The AoA $\varphi^a_{n,s}$ w.r.t. the ath antenna's local coordinate system and the distance $d^a_{n,s}$ to the ath antenna's phase center can be easily calculated from $d_{n,s}$ and $\varphi_{n,s}$ given known array geometry as shown in [8].

A. RSS Model and RSSD model

At time n, the RSS (in dBm) obtained at the ath antenna of sth anchor is given as

$$P^a_{n,s} \triangleq P_{0,s} + G_{\mathrm{Rx}}(\varphi^a_{n,s}) - 10\eta_{n,s}\log_{10}\left(\frac{d^a_{n,s}}{d_0}\right) + S^a_{n,s} + n^a_{n,s}\,, \quad (1)$$

according to the path-loss model [5]. The first term on the right side $P_{0,s}$ accounts for the transmit power P_{Tx} (in dBm), the transmit antenna gain G_{Tx} and the path loss $L_{\mathrm{ref},s}(d_0)$ at the reference distance $d_0 = 1\,\mathrm{m}$, i.e., $P_{0,s} = P_{\mathrm{Tx}} + G_{\mathrm{Tx}} + L_{\mathrm{ref},s}(d_0)$, $L_{\mathrm{ref},s}(d_0) = 20\log_{10}(\frac{\lambda}{4\pi}) - 10\eta_{n,s}\log_{10}(d_0)$, and λ is the wavelength. Furthermore, $G_{\mathrm{Rx}}(\varphi^a_{n,s})$ is the receive antenna gain at angle $\varphi^a_{n,s}$, $\eta_{n,s}$ is the PLE, and $S^a_{n,s} \sim \mathcal{N}(0,\, \sigma^2_{\mathrm{S}})$ models the log-normal shadow fading, which is independent and identically distributed (iid) across n and s. The shadow fading processes at adjacent antennas of each anchor are highly correlated and the correlation is denoted by C_{LSF}. We assume that P_{Tx} and G_{Tx} are known; $\eta_{n,s}$ is time-varying, unknown and independent across n and s. Here, the small scale fading and the measurement noise are jointly modeled using a zero-mean and Gaussian distribution that is iid across n, s and a, i.e., $n^a_{n,s} \sim \mathcal{N}(0,\, \sigma^2_{\mathrm{n}})$, with variance σ^2_{n}.

Based on (1), the RSSD measurement between two adjacent antennas of the jth anchor node at time n is modeled as [8]

$$P^{(r_1,r_2)}_{\Delta,n,s} \triangleq G^{(r_1,r_2)}_{\Delta,n,s}(\varphi_{n,s}) + \omega^{(r_1,r_2)}_{n,s}, \quad (2)$$

where the first term $G^{(r_1,r_2)}_{\Delta,n,s}(\varphi_{n,s})$ represents the antenna gain difference, given as $G^{(r_1,r_2)}_{\Delta,n,s}(\varphi_{n,s}) = G_{\mathrm{Rx}}(\varphi^{r_1}_{n,s}) - G_{\mathrm{Rx}}(\varphi^{r_2}_{n,s})$, with $\{r_1, r_2\} \in \mathcal{A}_s$, and $r_1 < r_2$. The noise term $\omega^{(r_1,r_2)}_{n,s}$ is approximated as the difference between two iid noise processes $n^{r_1}_{n,s}$ and $n^{r_2}_{n,s}$, thus $\omega^{(r_1,r_2)}_{n,s} \sim \mathcal{N}(0,\, 2\sigma^2_{\mathrm{n}})$.

The models (1) and (2) provide nonlinear mappings from the hidden state $\boldsymbol{x}_n$ of the target to RSS and RSSD observations, which enables the proposed algorithm to infer and fuse the distance and AoA information for target localization.

B. Inference Problem

In reality, it happens that at some time instances only a subset of antennas of each anchor, i.e., $\mathcal{K}_{n,s} \subseteq \mathcal{A}_s$, provide valid RSS measurements. Hence, the number $K_{n,s} = |\mathcal{K}_{n,s}|$ of RSS measurements $z^k_{n,s}$, $k \in \mathcal{K}_{n,s} \triangleq \{1, \cdots, K_{n,s}\}$ is time-varying. Accordingly, the RSSD measurement $z^l_{\mathrm{D},n,s}$ with $l \in \mathcal{L}_{n,s} \triangleq \{1, \cdots, L_{n,s}\}$ and $L_{n,s} = K_{n,s} - 1$ is obtained by taking the difference between RSS measurements from antenna pairs with adjacent indices, i.e., $\{r^l_1, r^l_2\} \in \mathcal{K}_{n,s}$, $r^l_1 < r^l_2$. At each time n, we assume that at least two antennas of each anchor provide RSS measurements. By stacking the measurement vectors $\boldsymbol{z}_{n,s} \triangleq [z^1_{n,s}, \ldots, z^{K_{n,s}}_{n,s}]^{\mathrm{T}}$ and $\boldsymbol{z}_{\mathrm{D},n,s} \triangleq [z^l_{\mathrm{D},n,s}, \ldots, z^{L_{n,s}}_{\mathrm{D},n,s}]^{\mathrm{T}}$ from all anchors, the full measurement vectors at time n are given as $\boldsymbol{z}_n \triangleq [\boldsymbol{z}^{\mathrm{T}}_{n,1}, \ldots, \boldsymbol{z}^{\mathrm{T}}_{n,S}]^{\mathrm{T}}$ and $\boldsymbol{z}_{\mathrm{D},n} \triangleq [\boldsymbol{z}^{\mathrm{T}}_{\mathrm{D},n,1}, \ldots, \boldsymbol{z}^{\mathrm{T}}_{\mathrm{D},n,S}]^{\mathrm{T}}$.

Our goal is to estimate of the target state $\boldsymbol{x}_n$, the path-loss exponents $\boldsymbol{\eta}_n = [\eta_{n,1}, \ldots, \eta_{n,S}]^{\mathrm{T}}$, using the past and present measurement vectors $\boldsymbol{z}_{1:n} \triangleq [\boldsymbol{z}^{\mathrm{T}}_1, \ldots, \boldsymbol{z}^{\mathrm{T}}_n]^{\mathrm{T}}$ and $\boldsymbol{z}_{\mathrm{D},1:n} \triangleq [\boldsymbol{z}^{\mathrm{T}}_{\mathrm{D},1}, \ldots, \boldsymbol{z}^{\mathrm{T}}_{\mathrm{D},n}]^{\mathrm{T}}$.

III. System Model and Statistical Formulation

A. Target Dynamics

For tracking a maneuvering target node, the IMM method [9]–[11] is used, which resolves the target motion uncertainty by using multiple dynamic models (i.e., modes) indexed by $m_n \in \mathcal{H} \triangleq \{1, \cdots, H\}$ at time n. The state-transition pdf of the target state $f_h(\boldsymbol{x}_n|\boldsymbol{x}_{n-1})$, $h \in \mathcal{H}$ when considering the hth mode is defined by the corresponding dynamic model. To account for the uniform motion as well as the maneuver of the target such as left/right turn, the nearly-constant velocity (NCV) model and the coordinated turn (CT) model [9] are used respectively. The NCV model is defined as $\boldsymbol{x}_n = \boldsymbol{F}_{\mathrm{NCV}}\boldsymbol{x}_{n-1} + \boldsymbol{\Gamma}\boldsymbol{\nu}_{n,h}$, where the matri $\boldsymbol{F}_{\mathrm{NCV}} \in \mathbb{R}^{4\times4}$ and $\boldsymbol{\Gamma} \in \mathbb{R}^{4\times2}$ are chosen as in [9, Section 6.3.2] with the sampling period ΔT. The driving process $\boldsymbol{\nu}_{n,h} \in \mathbb{R}^{2\times1}$ is iid across n and h, zero-mean and Gaussian with covariance matrix $\sigma^2_h \boldsymbol{I}_2$, $\boldsymbol{I}_2$ denotes a 2×2 diagonal matrix, and σ_h represents the average speed increment along x or y axis during the sampling period ΔT. Furthermore, the turn of a target is modeled with the CT model, characterized by a constant turn rate Ω_h and a (nearly) constant speed, i.e., $\boldsymbol{x}_n = \boldsymbol{F}_{\mathrm{CT}}(\Omega_h)\boldsymbol{x}_{n-1} + \boldsymbol{\Gamma}\boldsymbol{\nu}_{n,h}$, the matrices $\boldsymbol{F}_{\mathrm{CT}}(\Omega_h) \in \mathbb{R}^{4\times4}$ are chosen as in [9, Section 11.7.1]. The dynamic mode (DM) index m_n is modeled as a random variable which evolve according to the first-order Markov chain with a constant transition matrix $\boldsymbol{P} \in [0,1]^{H\times H}$ over time, where $[0,1]^{H\times H}$ denotes a $H \times H$ matrix with entries between 0 and 1. The DM transition probability mass function (pmf) of m_n is given by $p(m_n = j|m_{n-1} = i) = [\boldsymbol{P}]_{i,j}$ for $i, j \in \mathcal{H}$. Note that $\sum_{j=1}^{H}[\boldsymbol{P}]_{i,j} = 1\ \forall\, i$. The target state $\boldsymbol{x}_n$ and the DM index m_n are assumed to jointly evolve according to a Markovian dynamic model. Furthermore, we assume that the state $\boldsymbol{x}_n$ is conditionally independent of m_{n-1} given $\boldsymbol{x}_{n-1}$ and m_n, and m_n is conditionally independent of $\boldsymbol{x}_{n-1}$ given m_{n-1}. Thus, the joint prior pdf $f(\boldsymbol{x}_{1:n}, \boldsymbol{m}_{1:n})$ of $\boldsymbol{x}_{1:n} \triangleq [\boldsymbol{x}^{\mathrm{T}}_1, \ldots, \boldsymbol{x}^{\mathrm{T}}_n]^{\mathrm{T}}$ and $\boldsymbol{m}_{1:n} \triangleq [m_1, \ldots, m_n]^{\mathrm{T}}$ can be factorized as

$$\begin{aligned} f(\boldsymbol{x}_{1:n}, \boldsymbol{m}_{1:n}) &= f(\boldsymbol{x}_0, m_0) \prod_{n'=1}^{n} f(\boldsymbol{x}_{n'}, m_{n'}|\boldsymbol{x}_{n'-1}, m_{n'-1}) \\ &= f(\boldsymbol{x}_0) f(m_0) \prod_{n'=1}^{n} f_{m_{n'}}(\boldsymbol{x}_{n'}|\boldsymbol{x}_{n'-1}) f(m_{n'}|m_{n'-1}), \end{aligned} \quad (3)$$

where $f_{m_n}(\boldsymbol{x}_n|\boldsymbol{x}_{n-1}) = f(\boldsymbol{x}_n|m_n, \boldsymbol{x}_{n-1})$, $f(\boldsymbol{x}_0)$ and $f(m_0)$ are the initial prior pdf and pmf, which are assumed to be uniform on their respective regions of interest (RoIs).

B. Likelihood Functions

We assume that the individual measurements inside vectors $\boldsymbol{z}_{n,s}$ and $\boldsymbol{z}_{\mathrm{D},n,s}$ are conditionally independent given the states $\boldsymbol{x}_n$ and $\eta_{n,s}$, and $\eta_{n,s}$ is independent of RSSD measurements $\boldsymbol{z}_{\mathrm{D},n,s}$. The conditional pdfs $h(z^k_{n,s}|\boldsymbol{x}_n,\eta_{n,s})$ and $h(z^l_{\mathrm{D},n,s}|\boldsymbol{x}_k)$ (i.e., likelihood functions) derived from (1) and (2) are given as

$$h(z^k_{n,s}|\boldsymbol{x}_n,\eta_{n,s}) = C_1 \exp\left\{-\frac{(z^k_{n,s}-s^k_{n,s})^2}{2(\sigma_{\mathrm{S}}^2+\sigma_{\mathrm{n}}^2)}\right\}, \tag{4}$$

$$h(z^l_{\mathrm{D},n,s}|\boldsymbol{x}_n) = C_2 \exp\left\{-\frac{(z^l_{\mathrm{D},n,s}-G^{(r_1^l,r_2^l)}_{\Delta,n,s}(\boldsymbol{x}_n))^2}{4\sigma_{\mathrm{n}}^2}\right\}, \tag{5}$$

where $s^k_{n,s} = P_{0,s} + G_{\mathrm{Rx}}(\varphi^k_{n,s}) - 10\eta_{n,s}\log_{10}\left(\frac{d^k_{n,s}}{d_0}\right)$, and $G^{(r_1^l,r_2^l)}_{\Delta,n,s}(\boldsymbol{x}_n)$ represents the nonlinear mapping from the hidden state $\boldsymbol{x}_n$ to an RSSD observation described in (2), with $C_1 = \left(2\pi(\sigma_{\mathrm{S}}^2+\sigma_{\mathrm{n}}^2)\right)^{-\frac{1}{2}}$, $C_2 = (4\pi\sigma_{\mathrm{n}}^2)^{-\frac{1}{2}}$.

IV. The Message Passing Localization Algorithm

A. State Estimation

The joint estimation of $\boldsymbol{x}_n$ and $\eta_{n,s}$ given the measurements $\boldsymbol{z}_{1:n}$ and $\boldsymbol{z}_{\mathrm{D},1:n}$ is formulated with a Bayesian model, where the joint posterior pdf $f(\boldsymbol{x}_{1:n}, m_{1:n}, \boldsymbol{\eta}_{1:n}|\boldsymbol{z}_{1:n}, \boldsymbol{z}_{\mathrm{D},1:n})$ can be factorized as

$$\begin{aligned}
&f(\boldsymbol{x}_{1:n}, m_{1:n}, \boldsymbol{\eta}_{1:n}|\boldsymbol{z}_{1:n}, \boldsymbol{z}_{\mathrm{D},1:n}) \\
&\propto f(\boldsymbol{z}_{1:n}, \boldsymbol{z}_{\mathrm{D},1:n}|\boldsymbol{x}_{1:n}, m_{1:n}, \boldsymbol{\eta}_{1:n}) f(\boldsymbol{x}_{1:n}, m_{1:n}, \boldsymbol{\eta}_{1:n}) \\
&= f(\boldsymbol{x}_0) f(m_0) \left(\prod_{s=1}^{S} f(\eta_{0,s})\right) \\
&\quad \times \prod_{n'=1}^{n} f_{m_{n'}}(\boldsymbol{x}_{n'}|\boldsymbol{x}_{n'-1}) f(m_{n'}|m_{n'-1}) \prod_{s=1}^{S} f(\eta_{n',s}|\eta_{n'-1,s}) \\
&\quad \times \prod_{k\in\mathcal{K}_{n',s}} h(z^k_{n',s}|\boldsymbol{x}_{n'},\eta_{n',s}) \prod_{l\in\mathcal{L}_{n',s}} h(z^l_{\mathrm{D},n',s}|\boldsymbol{x}_{n'}),
\end{aligned} \tag{6}$$

according to the Bayes' rule and independence assumptions over the prior pdfs, state-transition pdfs, and the likelihood functions.

Based on the marginal posterior pdfs $f(\boldsymbol{x}_n|\boldsymbol{z}_{1:n}, \boldsymbol{z}_{\mathrm{D},1:n})$ and $f(\eta_{n,s}|\boldsymbol{z}_{1:n})$, the Bayesian estimation of the target state $\boldsymbol{x}_n$, the PLEs $\eta_{n,s}$ can be approximately calculated by means of the minimum mean square error (MMSE) estimator [12], given as

$$\hat{\boldsymbol{x}}_n^{\mathrm{MMSE}} \triangleq \int \boldsymbol{x}_n f(\boldsymbol{x}_n|\boldsymbol{z}_{1:n}, \boldsymbol{z}_{\mathrm{D},1:n})\mathrm{d}\boldsymbol{x}_n, \tag{7}$$

$$\hat{\eta}_{n,s}^{\mathrm{MMSE}} \triangleq \int \eta_{n,s} f(\eta_{n,s}|\boldsymbol{z}_{1:n})\mathrm{d}\eta_{n,s}. \tag{8}$$

B. Message Passing Algorithm

The marginal posterior pdfs $f(\boldsymbol{x}_n|\boldsymbol{z}_{1:n}, \boldsymbol{z}_{\mathrm{D},1:n})$ and $f(\eta_{n,s}|\boldsymbol{z}_{1:n})$ are obtained by running massage passing on the factor graph (Fig. 1) representing the factorization of the joint posterior pdf $f(\boldsymbol{x}_{1:n}, m_{1:n}, \boldsymbol{\eta}_{1:n}|\boldsymbol{z}_{1:n}, \boldsymbol{z}_{\mathrm{D},1:n})$ (6). Following

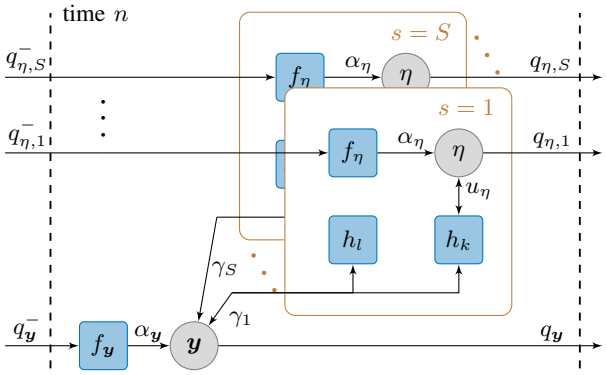

Fig. 1: Factor graph representation of the factorized joint posterior pdf (6), shown for time n. For simplicity, the joint vector of $\boldsymbol{x}_n$ and m_n are denoted as $\boldsymbol{y}_n = [\boldsymbol{x}_n, m_n]^{\mathrm{T}}$, the time indices are omitted and the following short notations are used: the beliefs calculated at the previous time $n-1$, $q^-_{\eta,s} = q(\eta_{n-1,s})$ and $q^-_{\boldsymbol{y}} = q(\boldsymbol{y}_{n-1})$; the state-transition pdfs $f_{\boldsymbol{y}} = f(\boldsymbol{y}_n|\boldsymbol{y}_{n-1})$ and $f_\eta = f(\eta_{n,s}|\eta_{n-1,s})$; the predicted messages $\alpha_{\boldsymbol{y}} = \alpha(\boldsymbol{y}_n)$ and $\alpha_\eta = \alpha(\eta_{n,s})$; the measurement-update messages $u_\eta = u(\eta_{n,s})$ and $\gamma_s = \gamma^s(\boldsymbol{y}_n)$; the likelihood functions related to RSS/RSSD measurements $h_k = h(z^k_{n,s}|\boldsymbol{x}_n,\eta_{n,s})$ and $h_l = h(z^l_{\mathrm{D},n,s}|\boldsymbol{x}_n)$; the beliefs that approximately representing the marginal posterior pdfs $q_{\eta,s} = q(\eta_{n,s})$ and $q_{\boldsymbol{y}} = q(\boldsymbol{y}_n)$.

the generic rules for calculating messages and beliefs introduced in [13], the following operations are performed at each time n:

1) *Prediction*: First, a prediction step is performed, and the messages $\alpha(\eta_{n,s})$ and $\alpha(\boldsymbol{x}_n, m_n)$ are calculated as

$$\alpha(\eta_{n,s}) = \int q(\eta_{n-1,s}) f(\eta_{n,s}|\eta_{n-1,s})\mathrm{d}\eta_{n-1,s}, \tag{9}$$

$$\begin{aligned}
\alpha(\boldsymbol{x}_n, m_n) = &\sum_{m_{n-1}\in\mathcal{H}} \int q(\boldsymbol{x}_{n-1}, m_{n-1}) f_{m_n}(\boldsymbol{x}_n|\boldsymbol{x}_{n-1}) \\
&\times f(m_n|m_{n-1})\mathrm{d}\boldsymbol{x}_{n-1},
\end{aligned} \tag{10}$$

where $q(\eta_{n-1,s})$ and $q(\boldsymbol{x}_{n-1}, m_{n-1})$ are calculated at time $n-1$.

2) *Measurement update*: In the measurement update step, the messages $u(\eta_{n,s})$ are calculated as

$$\begin{aligned}
u(\eta_{n,s}) = &\sum_{m_n\in\mathcal{H}} \int \alpha(\boldsymbol{x}_n, m_n) \\
&\times \prod_{k\in\mathcal{K}_{n,s}} h(z^k_{n,s}|\boldsymbol{x}_n,\eta_{n,s})\mathrm{d}\boldsymbol{x}_n,
\end{aligned} \tag{11}$$

and the message $\gamma^s(\boldsymbol{x}_n, m_n)$ from each anchor is given by

$$\gamma^s(\boldsymbol{x}_n, m_n) = \beta^s(\boldsymbol{x}_n, m_n)\beta^s_{\mathrm{D}}(\boldsymbol{x}_n, m_n), \tag{12}$$

where $\beta^s(\boldsymbol{x}_n, m_n)$ is the message passed form the factor node $h(z^l_{n,s}|\boldsymbol{x}_n,\eta_{n,s})$ to the variable node $\boldsymbol{x}_n$, given by

$$\beta^s(\boldsymbol{x}_n, m_n) = \int \alpha(\eta_{n,s}) \prod_{k\in\mathcal{K}_{n,s}} h(z^k_{n,s}|\boldsymbol{x}_n,\eta_{n,s})\mathrm{d}\eta_{n,s}, \tag{13}$$

and $\beta_{\mathrm{D}}^{s}(\boldsymbol{x}_n, m_n)$ is the message passed form the factor node $h(z_{\mathrm{D},n,s}^{l}|\boldsymbol{x}_n)$ to the variable node $\boldsymbol{x}_n$, given by

$$\beta_{\mathrm{D}}^{s}(\boldsymbol{x}_n, m_n) = \prod_{l \in \mathcal{L}_{n,s}} h(z_{\mathrm{D},n,s}^{l}|\boldsymbol{x}_n). \tag{14}$$

3) *Belief calculation*: Finally, the beliefs $q(\eta_{n,s})$ approximating the marginal posterior pdfs $f(\eta_{n,s}|\boldsymbol{z}_{1:n})$ are calculated as

$$q(\eta_{n,s}) = \alpha(\eta_{n,s})u(\eta_{n,s}). \tag{15}$$

Furthermore, the belief $q(\boldsymbol{x}_n, m_n)$ approximating the the marginal posterior pdf $f(\boldsymbol{x}_n, m_n|\boldsymbol{z}_{1:n}, \boldsymbol{z}_{\mathrm{D},1:n})$ is calculated as

$$q(\boldsymbol{x}_n, m_n) = \alpha(\boldsymbol{x}_n, m_n) \prod_{s=1}^{S} \gamma^{s}(\boldsymbol{x}_n, m_n). \tag{16}$$

Finally, the belief $q(\boldsymbol{x}_n)$ and $q(m_n)$ approximating $p(\boldsymbol{x}_n|\boldsymbol{z}_{1:n}, \boldsymbol{z}_{\mathrm{D},1:n})$ and $p(m_n|\boldsymbol{z}_{1:n}, \boldsymbol{z}_{\mathrm{D},1:n})$ are calculated as $q(\boldsymbol{x}_n) = \int q(\boldsymbol{x}_n, m_n)\mathrm{d}m_n$ and $q(m_n) = \int q(\boldsymbol{x}_n, m_n)\mathrm{d}\boldsymbol{x}_n$.

4) *Particle-based implementation*: A sequential Monte Carlo (particle-based) implementation [11], [14] is used to represent the messages and beliefs presented above. Furthermore, a "stacked state" [15] which comprises the target state and the PLE state is used in the implementation. Hence, the resulting complexity scales linearly in the number of particles, in the number of measurements per anchor, and quadratically in the number of mode number H.

V. Performance Evaluation

We validate the proposed message passing based localization algorithm using both synthetic and real measured RSS datasets. The work in [8] which exploits AoA information from RSSD measurements for target tracking is used as a reference method. Note that in [8] a single dynamic model is used. To remove the influence of difference target dynamic models on the results in two methods and make a fair comparison, we extend the algorithm in [8] with the IMM method introduced in Section (III-A) and keep the same setup on the DM modes. For simplicity, the two methods above will be briefly referred to as "MP-tracking" and "AoA-tracking" in what follows.

A. Measurement and Simulation Setup

The synthetic datasets are generated according to the setup of real outdoor measurement, which is described as follows: A LoRa based network [1] is used in our experimental setup. As shown in Fig. 2, the target node is equipped with an omnidirectional antenna with known transmit power of 14 dBm. Two anchor nodes are used, which are equipped with four and three directional antennas respectively, i.e., $A_1 = 4$ and $A_2 = 3$, and each receive antenna is connected with a gateway as shown in Fig. 2c. The gateways act as bidirectional relays between the target node and a network server, in

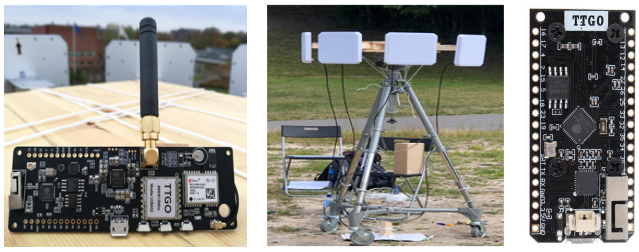

(a) (b) (c)

Fig. 2: Experimental setup: (a) target node: TTGO T-Beam module, (b) anchor node: four 9 dBi circular antennas are used, and each antenna is connected to a TTGO gateway shown in (c).

which the messages like GPS "ground truth" and RSS values are decoded. The distance between the phase centers and the orientation difference of two adjacent antennas are one wavelength and 45 degrees, respectively. One of the receive antenna beam patterns is measured and assumed to be the same for the rest of the antennas. The system is operating at the carrier frequency 868 MHz, with a bandwidth of 125 kHz. The maximum spreading factor 12 is used to achieve the longest working range, however at the cost of low data and package rate. The gateways are listening to several different channels, every 6 seconds one packet is received at each antenna.

The following parameters and simulation setup are used for both synthetic and real measurements. We assume that the initial target position is roughly known, and the particles for the initial target state are drawn from a 4-D uniform distribution with the center at $[\boldsymbol{p}_1\, 0\, 0]$, where $\boldsymbol{p}_1$ denotes the ground truth position of the target at time $n = 1$, and the supports for the position and velocity are given as $[-50,\, 50]\,\mathrm{m}$ and $[-1,\, 1]\,\mathrm{m/s}$, respectively. The state-transition pdfs of the target state $f_h(\boldsymbol{x}_n|\boldsymbol{x}_{n-1})$ under three DM modes are defined by the following models respectively: 1) CT model for right turn with $\Omega_1 = -5\,\mathrm{deg/s}$, $\sigma_1 = 0.001\,\mathrm{m/s^2}$; 2) NCV model with $\sigma_2 = 0.001\,\mathrm{m/s^2}$; 3) CT model for left turn with $\Omega_3 = 5\,\mathrm{deg/s}$ and $\sigma_3 = 0.001\,\mathrm{m/s^2}$. The sampling period $\Delta T = 6\,\mathrm{s}$. The DM transition probabilities are chosen as $[\boldsymbol{P}]_{1,1} = [\boldsymbol{P}]_{3,3} = 0.95$, $[\boldsymbol{P}]_{2,2} = 0.96$, $[\boldsymbol{P}]_{2,1} = [\boldsymbol{P}]_{2,3} = 0.02$, $[\boldsymbol{P}]_{1,2} = [\boldsymbol{P}]_{3,2} = 0.04$, and $[\boldsymbol{P}]_{1,3} = [\boldsymbol{P}]_{3,1} = 0.01$. Besides, the state-transition pdfs of the path-loss exponents $f(\eta_{n,s}|\eta_{n-1,s})$ are given as Gaussian distributions with noise standard deviations $\sigma_\eta = 0.07$. The particles for the initial PLE state $\eta_{0,s}$ are drawn from a uniform distribution on $[1,\, 5]$. The pdf of each variable state is represented by 5000 particles.

B. Synthetic Measurements

Using the GPS positions of the anchors and the target at each time n, we calculate the ground truth distances and AoAs, and then apply them in model (1) to generate the synthetic RSS measurements. Furthermore, the ground truth PLEs are set according to the true propagation conditions and the estimates from the real meausrments as shown in Fig. 8. For each simulation run, the shadow fading and Gaussian noise processes are generated at each time n under one of the two setups: 1) *setup*-1: $\sigma_{\mathrm{S}} = 2\,\mathrm{dB}$, $\sigma_{\mathrm{n}} = 0.8\,\mathrm{dB}$,

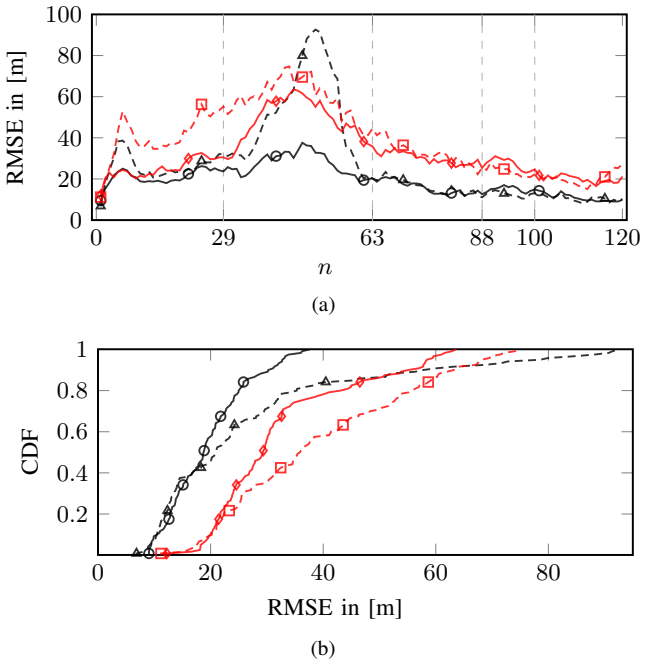

Fig. 3: Results for synthetic data. (a) Target position RMSEs. (b) Empirical CDFs of the position RMSEs. *setup*-1: MP-tracking (—○—), AoA-tracking (- -△- -), *setup*-2: MP-tracking (—◇—), AoA-tracking (- -□- -). The vertical dashed lines highlight the times around which the target node performs sharp turns as shown in Fig. 6.

$c_{\mathrm{LSF}} = 0.9$; 2) *setup*-2 (based on the statistics from real measurements): $\sigma_{\mathrm{S}} = 4\,\mathrm{dB}$, $\sigma_{\mathrm{n}} = 1\,\mathrm{dB}$, $C_{\mathrm{LSF}} = 0.8$. The noise standard deviations σ_{S} are σ_{n} are assumed to be known in the simulations. In total, we performed 100 Monte-Carlo (MC) simulation runs for each setup.

Fig. 3a depicts the target position RMSEs of MP-tracking and AoA-tracking methods, and the corresponding empirical cumulative distribution function (CDF) are given in Fig. 3b. By exploiting both range and angle information from RSS measurements, it shows that the MP-tracking method achieves lower RMSEs then the AoA-tracking method mostly. More specifically, the maximum RMSEs for MP-tracking are below 40 m and 65 m for *setup*-1 and *setup*-2, while the values are 95 m and 75 m for AoA-tracking. Fig. 4 shows the averaged PLE estimates over 100 MC runs. It can be seen that the PLE estimates of MP-tracking represent the ground truth well in both setups, which proves that MP-tracking can adapt to dynamic propagation conditions. Moreover, the averaged DM mode beliefs are given in Fig. 5. As can be observed, whenever the target performs a sharp turn, the belief of the corresponding DM mode increases and tends to be dominant, and the smooth movement in between those turns is captured by the NCV model, as expected.

C. Real Measurements

The real RSS measurements are collected at the campus of Lund University, Sweden, as shown in Fig. 6. Two anchor nodes are placed on two building roofs, which are around 20 m above the ground. The target node is carried by a person walking along a predefined trajectory at a speed around 1 m/s.

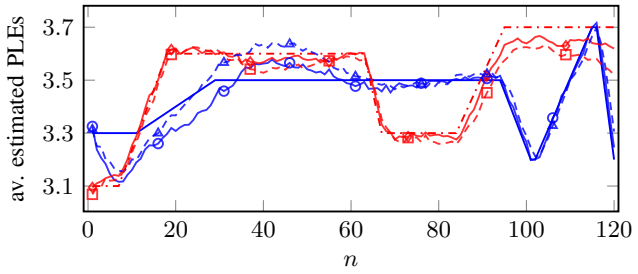

Fig. 4: Results for synthetic data using MP-tracking. Averaged PLE estimates for (a) anchor 1: ground truth (——), *setup*-1 (—○—), *setup*-2 (- -△- -); (b) anchor 2: ground truth (-·-·-), *setup*-1 (—◇—), *setup*-2 (- -□- -).

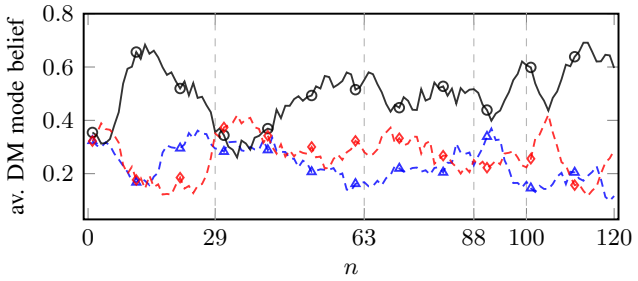

Fig. 5: Results for synthetic data using MP-tracking. Averaged DM mode beliefs for *setup*-2. (a) CT model for right turn (- -△- -). (b) NCV (—○—). (C) CT model for left turn (- -◇- -).

Every 6 seconds, the movement is paused and we collect around three samples at each antenna. Still, at a few positions only a subset of antennas provide valid RSS measurements. In total, there are $N = 120$ sample time instances. In Fig. 6, we mark the time instances where the target performs sharp turns with brown circle. In the simulations, we assume the noise standard deviations for the shadow fading and Gaussian noise processes to be $\sigma_{\mathrm{S}} = 4\,\mathrm{dB}$, $\sigma_{\mathrm{n}} = 1\,\mathrm{dB}$. We evaluate the performance both for the averaged and non-averaged measurements. For the first case, the RSS measurements collected at each antenna are averaged. For the second case, we randomly pick one measurement from each antenna at each time, and in total 50 MC simulation runs are performed.

As shown in Fig. 7, the MP-tracking algorithm outperforms the AoA-tracking algorithm especially when non-averaged measurements are used. Furthermore, the true propagation conditions from the target to each anchor are denoted with line-of-sight (LoS), obstructed-LoS (OLoS) where the direct propagation is blocked by trees, and non-LoS (NLoS) where the direct propagation is blocked by one or two buildings (abbreviated as bul.). As shown in Fig. 8, the PLE estimates well capture the dynamics of the true propagation conditions to each anchor.

VI. Conclusion

We proposed a localization algorithm that exploits both range and angle information from non-coherent RSS measurements for IoT networks. Results using real outdoor measurements show that the proposed algorithm can adapt to dynamic propagation conditions, and improve the localization accuracy compared to the method which exploits single geometric

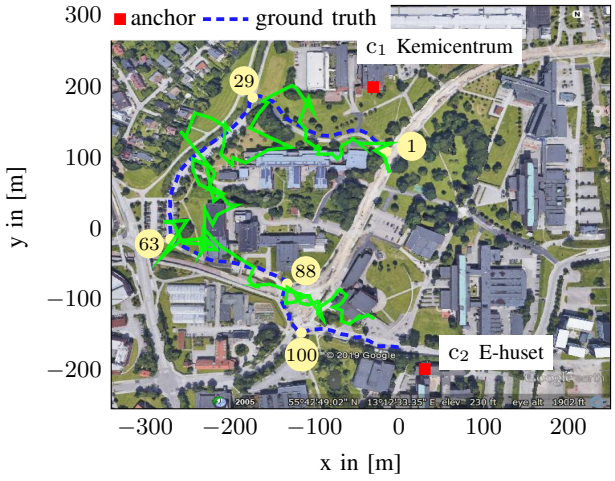

Fig. 6: Picture of the outdoor measurement environment, Lund University, Sweden. Background map: © 2019 Google

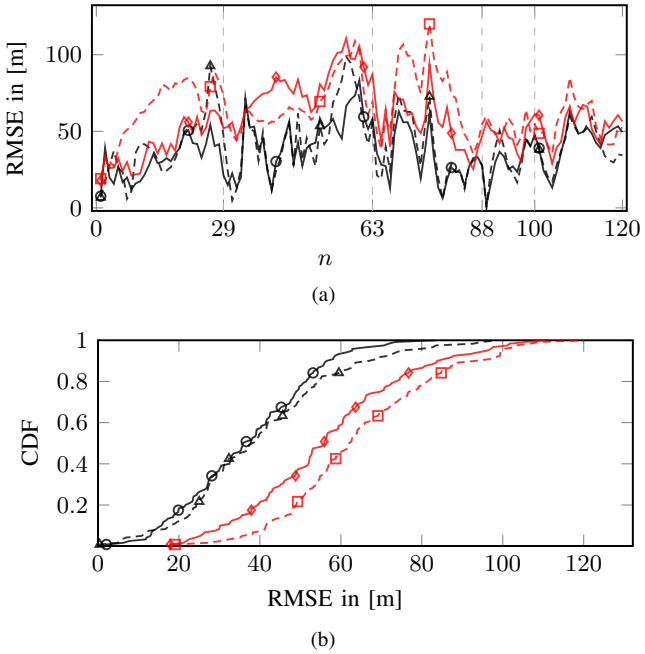

Fig. 7: Results for real data. (a) Target position RMSEs. (b) Empirical CDFs of the position RMSEs. For averaged RSS measurements: MP-tracking (—o—), AoA-tracking (- -△- -), For single RSS measurement: MP-tracking (—◇—), AoA-tracking (- -□- -).

feature. Moreover, the proposed algorithm is compatible with many existing low cost IoT technologies and different antenna array configurations.

VII. Acknowledgment

This work was supported in part by the Swedish Research Council (VR), in part by the strategic research area ELLIIT and in part by the TU Graz.

References

[1] M. Centenaro, L. Vangelista, A. Zanella, and M. Zorzi, "Long-range communications in unlicensed bands: the rising stars in the IoT and smart city scenarios," *IEEE Wirel. Commun.*, vol. 23, no. 5, pp. 60–67, Oct. 2016.

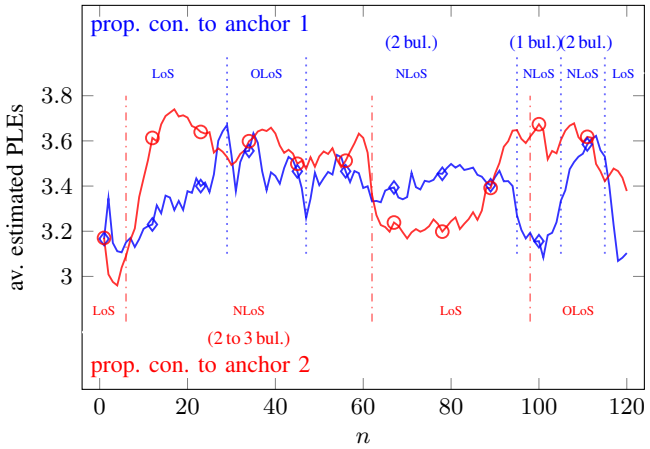

Fig. 8: Results for real data. PLE estimation from anchor 1 (—◇—) and from anchor 2 (—o—). The propagation conditions from the target node to anchor 1 and anchor 2 are labeled in blue and red colors respectively. Furthermore, the vertical lines (·····) and (-·-·-) highlight the time instances around which the propagation conditions to anchor 1 and anchor 2 change respectively.

[2] B. Mager, P. Lundrigan, and N. Patwari, "Fingerprint-based device-free localization performance in changing environments," *IEEE J. Sel. Areas Commun.*, vol. 33, no. 11, pp. 2429–2438, Nov. 2015.

[3] S. Yiu, M. Dashti, H. Claussen, and F. Perez-Cruz, "Wireless RSSI fingerprinting localization," *Signal Process.*, vol. 131, pp. 235 – 244, Jul. 2017.

[4] S. Tomic, M. Beko, and R. Dinis, "RSS-based localization in wireless sensor networks using convex relaxation: Noncooperative and cooperative schemes," *IEEE Trans. Veh. Technol.*, vol. 64, no. 5, pp. 2037–2050, May. 2015.

[5] A. Zanella, "Best practice in RSS measurements and ranging," *IEEE Commun. Surveys Tuts.*, vol. 18, no. 4, pp. 2662–2686, Fourthquarter 2016.

[6] "LoRa alliance geolocation whitepaper," *LoRa Alliance*, 2018. [Online]. Available: https://lora-alliance.org/resource-hub/lora-alliance-geolocation-whitepaper

[7] J. Jiang, C. Lin, F. Lin, and S. Huang, "ALRD: AoA localization with RSSI differences of directional antennas for wireless sensor networks," in *Int. Conf. on Inform. Soc. (i-Society 2012)*, June 2012, pp. 304–309.

[8] X. Li, M. A. Nasa, F. Rezaei, and F. Tufvesson, "Target tracking using signal strength differences for long-range IoT networks," in *IEEE Int. Conf. on Commun. Workshops (ICCW)*, June 2020.

[9] Y. Bar-Shalom, T. Kirubarajan, and X. R. Li, *Estimation with Applications to Tracking and Navigation*. New York, NY, USA: Wiley, 2002.

[10] E. Mazor, A. Averbuch, Y. Bar-Shalom, and J. Dayan, "Interacting multiple model methods in target tracking: a survey," *IEEE Trans. Aerosp. Electron. Syst.*, vol. 34, no. 1, pp. 103–123, Jan. 1998.

[11] G. Soldi, F. Meyer, P. Braca, and F. Hlawatsch, "Self-tuning algorithms for multisensor-multitarget tracking using belief propagation," *IEEE Trans. Signal Process.*, vol. 67, no. 15, pp. 3922–3937, Aug. 2019.

[12] S. M. Kay, *Fundamentals of Statistical Signal Processing: Estimation Theory*. Upper Saddle River, NJ, USA: Prentice-Hall, Inc., 1993.

[13] F. Kschischang, B. Frey, and H.-A. Loeliger, "Factor graphs and the sum-product algorithm," *IEEE Trans. Inf. Theory*, vol. 47, no. 2, pp. 498–519, Feb. 2001.

[14] M. S. Arulampalam, S. Maskell, N. Gordon, and T. Clapp, "A tutorial on particle filters for online nonlinear/non-Gaussian Bayesian tracking," *IEEE Trans. Signal Process.*, vol. 50, no. 2, pp. 174–188, Feb. 2002.

[15] F. Meyer, O. Hlinka, H. Wymeersch, E. Riegler, and F. Hlawatsch, "Distributed localization and tracking of mobile networks including noncooperative objects," *IEEE Trans. Signal Inf. Process. Net.*, Mar. 2016.